

学位論文

Trpm7 protein contributes to intercellular junction formation in mouse urothelium

(Trpm7 蛋白のマウス尿路上皮細胞間結合の形成への関与)

旭川医科大学大学院医学系研究科博士課程医学専攻

渡邊 成樹

(鈴木 喜郎 内田 邦敏 宮崎 直幸 村田 和義 松本 成史 柿崎 秀宏 富永 真琴)

Trpm7 Protein Contributes to Intercellular Junction Formation in Mouse Urothelium*

Received for publication, May 29, 2015, and in revised form, October 15, 2015. Published, JBC Papers in Press, October 26, 2015, DOI 10.1074/jbc.M115.667899

Masaki Watanabe^{‡§}, Yoshiro Suzuki^{‡¶1}, Kunitoshi Uchida^{‡¶1}, Naoyuki Miyazaki^{||}, Kazuyoshi Murata^{||}, Seiji Matsumoto[§], Hidehiro Kakizaki[§], and Makoto Tominaga^{‡¶1,2}

From the [‡]Division of Cell Signaling, Okazaki Institute for Integrative Bioscience (National Institute for Physiological Sciences), National Institutes of Natural Sciences, Okazaki 444-8787, the [§]Department of Renal and Urologic Surgery, Asahikawa Medical University, Asahikawa 078-8510, the ^{¶1}Department of Physiological Sciences, SOKENDAI (The Graduate University for Advanced Studies), Okazaki 444-8787, and the ^{||}National Institute for Physiological Sciences, National Institutes of Natural Sciences, Okazaki 444-8585, Japan

Background: Transient receptor potential melastatin 7 (Trpm7) is a Ca²⁺-permeable channel with a kinase domain that is implicated in cell migration and adhesion.

Results: Urothelium-specific *Trpm7* knock-out caused immature intercellular junctions, inflammation, and smaller voided volume.

Conclusion: Trpm7 contributes to the intercellular junction formation in the urothelium.

Significance: These findings might provide the first evidence for the significance of Trpm7 in bladder function *in vivo*.

Trpm7 is a divalent cation-permeable channel that has been reported to be involved in magnesium homeostasis as well as cellular adhesion and migration. We generated urothelium-specific *Trpm7* knock-out (KO) mice to reveal the function of Trpm7 *in vivo*. A *Trpm7* KO was induced by tamoxifen and was confirmed by genomic PCR and immunohistochemistry. By using patch clamp recordings in primary urothelial cells, we observed that Mg²⁺-inhibitable cation currents as well as acid-inducible currents were significantly smaller in *Trpm7* KO urothelial cells than in cells from control mice. Assessment of voiding behavior indicated a significantly smaller voided volume in *Trpm7* KO mice (mean voided volume 0.28 ± 0.08 g in KO mice and 0.36 ± 0.04 g in control mice, *p* < 0.05, *n* = 6–8). Histological analysis showed partial but substantial edema in the submucosal layer of *Trpm7* KO mice, most likely due to inflammation. The expression of proinflammatory cytokines TNF- α and IL-1 β was significantly higher in *Trpm7* KO bladders than in controls. In transmission electron microscopic analysis, immature intercellular junctions were observed in *Trpm7* KO urothelium but not in control mice. These results suggest that Trpm7 is involved in the formation of intercellular junctions in mouse urothelium. Immature intercellular junctions in *Trpm7* knock-out mice might lead to a disruption of barrier

function resulting in inflammation and hypersensitive bladder afferent nerves that may affect voiding behavior *in vivo*.

Transient receptor potential (TRP)³ channels play critical roles in sensing environmental stimuli, including physical and chemical stimuli (temperature and pH), and conducting that information into cells (1–4). Trpm7 (transient receptor potential melastatin 7) and its closest homolog Trpm6 are unique members of the TRP channel family because they have a kinase domain within the same polypeptide (5). Trpm7 is a ubiquitously expressed non-selective cation channel that has been reported to be important for Mg²⁺ homeostasis. Although Trpm7 might indeed be involved in total body Mg²⁺ homeostasis (6), there is growing evidence suggesting that Trpm7 is not a determinant for intracellular Mg²⁺ content (7, 8). In contrast, it has been shown that Trpm7 has a crucial role in cancer cell migration, including formation of focal adhesions as well as adherence junctions (9–12). Nonetheless, the physiological significance of Trpm7 *in vivo* remains unknown.

To investigate the significance of Trpm7 *in vivo*, we focused on the epithelium in the urinary bladder (urothelium), the architecture of which is dynamically rearranged during the storage and emptying of urine (13, 14). Although the functional expression of Trpm7 has been reported in the urothelium (15), its physiological role remains unclear. We attempted for the first time to generate urothelium-specific *Trpm7* knock-out (KO) mice, and we found that the endogenous acid-sensitive currents were derived at least in part from Trpm7. More importantly, *Trpm7* KO mice exhibited a smaller voided volume of urine. Indeed, interstitial inflammation was observed in *Trpm7* KO bladders. With electron microscopy, we observed that intercellular junctions were impaired in *Trpm7* KO urothelium. These results suggest that Trpm7 is essential for the for-

* This work was supported by Ministry of Education, Culture, Sports, Science, and Technology in Japan Grant 23249012 (to M. T.). The authors declare that they have no conflicts of interest with the contents of this article.

¹ To whom correspondence may be addressed: Division of Cell Signaling, Okazaki Institute for Integrative Bioscience (National Institute for Physiological Sciences), National Institutes of Natural Sciences, 5-1, Higashiyama, Myodaiji, Okazaki 444-8787, Japan. Tel.: 81-564-59-5286; Fax: 81-564-59-5285; E-mail: yoshiro@nips.ac.jp.

² To whom correspondence may be addressed: Division of Cell Signaling, Okazaki Institute for Integrative Bioscience (National Institute for Physiological Sciences), National Institutes of Natural Sciences, 5-1, Higashiyama, Myodaiji, Okazaki 444-8787, Japan. Tel.: 81-564-59-5286; Fax: 81-564-59-5285; E-mail: tominaga@nips.ac.jp.

³ The abbreviations used are: TRP, transient receptor potential; fl, floxed; eGFP, enhanced GFP; pF, picofarad.

mation of the intercellular junctions in the urothelium. Abnormal intercellular junctions could lead to a barrier disruption and inflammation that could impair bladder function *in vivo*.

Experimental Procedures

RT-PCR—Urinary bladder tissue or primary urothelial cells were extracted with a Sepasol Super G kit (20–40 mg/500 μ l of solution, Nacalai, Japan). After homogenizing with a disposable Potter-type homogenizer, chloroform was added and incubated for 3 min. The mixture was then centrifuged at 10,000 \times *g* for 15 min at 4 °C. The upper layer was treated with an equal volume of 2-propanol and incubated for 10 min. After centrifugation at 10,000 \times *g* at 4 °C for 10 min, the pellet was washed with 75% ethanol and then dissolved with nuclease-free water. After measuring the absorbance, the total RNA solution (1 μ g/ μ l) was stored at –80 °C prior to use. Reverse transcription was performed using a Superscript III kit (Invitrogen). One μ g of the total RNA was mixed with 1 μ l of oligo(dT)₂₀ (50 μ M) and 5 μ l of dNTPs (2.5 mM) and incubated at 65 °C for 5 min. After the annealing, Superscript III reverse transcriptase was added in 4 μ l of First-Strand buffer, 1 μ l of DTT (0.1 M), and 1 μ l of RNase OUT (Invitrogen) and incubated at 50 °C for 1 h. After heat inactivation (70 °C for 15 min), the single strand cDNA solution was stored at –20 °C until use.

The PCR was performed using an EmeraldAmp kit (Takara, Japan). As a template, the above mentioned cDNA sample was used. As a positive control, a vector construct with partial cDNA of each molecule was used with a 1:50 dilution. Primer sequences were as follows: *Trpm7*-forward, 5'-CCTCATGAA-GACCATTTTCTAA, and *Trpm7*-reverse, 5'-ACAACGTGTA-ACCTTCCTCACAG; β -actin-forward, TGTTACCAACTGGACGACA, and β -actin-reverse: AAGGAAGGCTGGA-AAAGAGC; *Upk3a*-forward, TCCCACTGAGCACCCTTTC, and *Upk3a*-reverse, AGCTTGCTGGAGAACACCTC; and *Acta2* (smooth muscle actin)-forward, AGCTTGCTGGAGAACACCTC, and *Acta2*-reverse, TGAAGTCAGTGTTCGATTTTCC. The PCR mix contained the template or control vector (1 μ l), EmeraldAmp PCR MasterMix (0.5 volume), and the above mentioned forward and reverse primers (1 μ l each, 10 pmol/ μ l). The reaction cycle was as follows: after incubation at 94 °C for 2 min, 35 cycles of denaturing (94 °C for 30 s), annealing (49 °C for *Trpm7*, 63 °C for β -actin, and 53 °C for *Upk3a* and 51 °C for *Acta2*) for 30 s, and elongation (72 °C for 1 min). After the cycle, the sample was incubated at 72 °C for 10 min. These PCR fragments were then visualized by agarose gel electrophoresis.

***Trpm7* Knock-out Mice**—*Trpm7*-floxed mice were generated as described previously (7) and maintained on the 129/SvEvTac background. According to previous papers on *Trpm7* KO mice (7, 8), global *Trpm7* disruption in mice leads to early embryonic lethality. To obtain conditional *Trpm7* KO mouse, the Cre-loxP system (16) was used. The *Upk3a*-GCE strain containing enhanced GFP-Cre-ERT2 expressed under the control of the *Upk3a* promoter was purchased from The Jackson Laboratory. Ten mg of tamoxifen (Sigma) was dissolved in 1 ml of corn oil (WAKO, Japan) at 65 °C for 1 h. Tamoxifen (50–100 μ g/g body weight) was administered intraperitoneally to the control group (*Trpm7*^{fl/fl}) or the *Trpm7* KO group (*Upk3a*-Cre;

Trpm7^{fl/fl}) once a week for 4 weeks. All the experiments were performed at least 7 days after the last injection. All animal care and experimental procedures were performed according to the National Institutes of Health and National Institute for Physiological Sciences guidelines.

Genotyping PCR—The urothelial layer was collected from anesthetized, tamoxifen-treated mice, after which the tissue was incubated with a lysis buffer (10 mM Tris-HCl, 200 mM NaCl, 5 mM EDTA, 0.2% SDS) containing proteinase K (0.5 μ g/ μ l, Sigma) at 55 °C overnight with shaking. After inactivation at 95 °C for 10 min, the genomic DNA solution was stored at –20 °C until use. The genomic PCR was performed using an EmeraldAmp kit (Takara, Japan) with the following primers: *Trpm7* exon 17-forward, 5'-GCCATCTCTCCTCTGGTTTT, and *Trpm7* exon 17-reverse, 5'-GATAGACTATATACTAGGTACATGG. The reaction mix contained genomic DNA (0.5 μ g), forward and reverse primers (each 1 μ l, 10 pmol/ μ l), and EmeraldAmp Master Mix (0.5 volume). The reaction was done with the following sequence: after incubation at 95 °C for 2 min, 35 cycles of denaturing (95 °C for 30 s), annealing (60 °C for 30 s), and elongation (72 °C for 1 min) were performed. These PCR fragments were then visualized by agarose gel electrophoresis.

Immunohistochemistry and Immunocytochemistry—The bladder tissue was resected from anesthetized mice and fixed in 10% buffered formaldehyde (Wako, Osaka, Japan). After further fixation for 24 h at 4 °C, the tissue was incubated twice with 30% sucrose in PBS for 24 h at 4 °C and then embedded with OCT compound (Sakura, Japan). The tissue block was stored at –80 °C until use. The sections were cut with a cryostat (CM3050S, Leica, Germany) with a 7- μ m thickness. Primary cultures of mouse urothelial cells were fixed with 10% buffered formaldehyde for 10 min and incubated twice with 30% sucrose in PBS for 24 h at 4 °C. The treated primary culture and the tissue sections were then washed three times with PBS and treated with 5% normal goat serum with 0.05% Triton X-100 (Sigma) in PBS for 30 min at room temperature. After the blocking treatment, the section and the cells were treated with diluted rabbit anti-human TRPM7 antibody (from Dr. Yasuo Mori, Kyoto University, Japan). The amino acid sequence of the epitope is identical between human and mice. It was used at a 1:500 dilution for immunohistochemistry and 1:50 for immunocytochemistry. Rabbit anti-eGFP antibody (Life Technologies, Inc.) was used at a 1:1000 dilution. Mouse anti-human cytokeratin 7 (CK7) antibody (CK7, Monosan, Netherlands) was used at a 1:50 dilution. After incubation with the primary antibody overnight at 4 °C, the sections or cells were washed three times with PBS containing 0.05% Triton X-100 and treated with secondary antibody (Alexa Fluor-conjugated, Molecular Probes) for 2 h at room temperature under dark conditions. DAPI was used for nuclear staining. After a 10-min incubation, sections and cells were washed and mounted with Fluoromount (DBS) and visualized by fluorescent microscopy (BZ9000, KEYENCE, Japan). The signal was semi-quantified by ImageJ software.

Primary Culture of Mouse Urothelial Cells—Following anesthesia, whole bladders were separated, and urothelial cells were prepared by the methods described previously with slight mod-

Functional Impairment of Urothelial Trpm7-Knock-out Bladder

ifications (17, 18). The everted bladder was incubated with papain (6 $\mu\text{l/ml}$) for 25 min at 37 °C with just one tapping for 15 min after incubation. The isolated urothelial cells were seeded on 12-mm diameter coverslips (Matsunami, Japan) coated with fibronectin (AGC Techno Glass Co., Ltd., Japan) and incubated in urothelium-dedicated culture medium (CNT-16; CELLn-TEC, Switzerland). Immunocytochemistry with an epithelial marker (cytokeratin 7) was performed to ascertain whether the cultured cells were urothelial cells (19).

Whole-cell Patch Clamp Recording in Primary Urothelial Cells—Whole-cell patch clamp recordings were performed 3–8 h after seeding freshly isolated urothelial cells. Primary urothelial cells on 12-mm diameter coverslips were mounted in a chamber. The control bath solution (300–310 mosmol/kg H_2O) contained 143 mM NaCl, 5 mM KCl, 5 mM HEPES, 10 mM glucose, 2 mM CaCl_2 , and 1 mM MgCl_2 (pH 7.4). The solution for observing the activity of Trpm7 contained 125 mM NaCl, 20 mM HEPES, 10 mM glucose, 5.1 mM CaCl_2 , 0 mM MgCl_2 , 5 mM EGTA, and 30 mM mannitol (pH 7.4). The solution for observing the response to an acid (pH 4) contained 125 mM NaCl, 20 mM MES, 10 mM glucose, 0.1 mM CaCl_2 , 0 mM MgCl_2 , 5 mM EGTA, and 30 mM mannitol (pH 4). To observe the effects of Mg^{2+} , 10 mM MgCl_2 was added to the bath while maintaining a constant osmolality by reducing the concentration of mannitol. The free Mg^{2+} or Ca^{2+} concentration was calculated with MAX chelator software. The pipette solution (300–305 mosmol/kg H_2O) contained 140 mM CsCl, 10 mM *O,O'*-bis-(2-aminophenyl)ethyleneglycol-*N,N,N',N'*-tetraacetic acid, and 10 mM HEPES (pH 7.3). The resistance of the pipette was around 7 megohms. Data were sampled at 10 kHz and filtered at 4 kHz for analysis (Axon 700B amplifier with pCLAMP software, Axon Instruments, Molecular Devices, Japan). Membrane potential was clamped at -60 mV, and voltage ramp-pulses from -100 to $+100$ mV (500 ms) were applied every 5 s. All experiments were performed at room temperature. Recording started at about 2 min after making a whole-cell configuration. When the increase of the current seemed to reach a plateau, 10 mM Mg^{2+} was applied for 30 s, and the inhibition of the current was analyzed as a magnesium-inhibitable current. For the measurement of the response to an acid, an acidic solution (pH 4) was applied for 30 s when the increase of the Trpm7-derived current seemed to reach a plateau. The data at -60 mV before and after application of the acidic solution were analyzed. Regarding the measurement of the Mg^{2+} inhibition in response to the acidic solution, the data before and after application of 10 mM Mg^{2+} were analyzed.

Study of Voiding Behavior—A study of voiding behavior was performed with free-moving mice that were awake. They were housed in modified metabolic cages (type 304 stainless steel, TECNIPLAST, Italy). Each mouse was placed in an individual metabolic cage under 12-h light-dark conditions. They could freely access water and food. The adaptation period was 4–7 days. Cages were located above an electronic balance (GX-06, A & D Instruments, Japan), and the weight of urine was directly measured by this device in real time. Most of the excrement was trapped by two metal filters. These filters were treated with a water-repellent finish so that almost all the urine could pass through these filters. Data were continuously recorded for 3–7

days with Powerlab software and analyzed with Labchart7 software. Total weight, total amount of urine for 24 h, and the weight of voided volume per micturition were calculated.

Histological Analysis—Tissue blocks were prepared as described under “Immunohistochemistry and Immunocytochemistry.” The sections were made with a cryostat (CM3050, Leica, Germany) with a thickness of 9 μm . The sections were fixed in 10% buffered formaldehyde (Wako, Japan) for 10 min, washed three times with PBS, and stained with Meyer’s hematoxylin solution (Wako, Japan) and eosin solution (Wako, Japan), followed by dehydration with 30, 70, 90, and 100% ethanol and then 100% xylene, each for 2 min. The dehydrated sections were then mounted with Permount (Fisher) and dried overnight. The tissue sections were analyzed by microscopy (BZ9000, KEYENCE, Japan). An edema score was determined for each section as described previously (20).

Cytokine Profiling—Total RNA from bladder was isolated, and cDNA was synthesized as described under “RT-PCR.” Real time PCR was performed with 10 μl of SYBR Master Mix Reagent (Takara, Japan), 0.25 μM specific primer sets (*Tnfa*, *Il1b*, *Il6*, *Il10*, *Il12*, *Il15*, *Il18*, and *Tgfb1*) as follows: mTNF α -F, 5'-CCCCAAAGGGATGAGAAGTT, and mTNF α -R, 5'-GTGGGTGAGGAGCACGTAGT; mIL1b-F, 5'-GGATGAGGACATGAGCACCT, and mIL1b-R, 5'-AGGCCACAGGTATTTGTCTCG; mIL6-F, 5'-TGTGCAATGGCAATTCTGAT, and mIL6-R, 5'-GGAAATGGGGTAGGAAGGA; mIL10-F, 5'-TGCTATGCTGCCTGCTCTTA, and mIL10-R, 5'-TCTCACCCAGGGAATTCAA; mIL12b-F, 5'-TGACACGCCTGAA-GAAGATG, and mIL12b-R, 5'-TCAGGGGAACTGCTACTGCT; mIL15F, 5'-CATTTTGGGCTGTGTGTCAGTG, and mIL15-R, 5'-TCTCCTCCAGCTCCTCACAT; mIL18-F, 5'-ACAACCTTTGGCCGACTTCAC, and mIL18-R, 5'-TGGATCCATTTCCCTCAAAGG; and mTGF β 1-F, 5'-TGAGTGGCTGTCTTTTGACG, and mTGF β 1-R, 5'-TCTCTGTGGAGCTGAAGCAA; and 1 μl of the prepared cDNA. Real time PCRs were performed using a StepOne analyzer (Life Technologies, Inc.). The temperature profile consisted of 40 cycles of denaturation at 95 °C for 15 s, annealing for 30 s, and elongation at 72 °C for 1 min. To discriminate specific and nonspecific amplifications, melting curve analysis was performed at the end of each PCR assay. To determine the starting cDNA amount, purified PCR products with known concentrations were serially diluted and used as standards.

Transmission Electron Microscopy—Transmission electron microscopic analysis was carried out as described previously with some modifications (21, 22). In the transmission electron microscopy study, female mice were used. Following anesthesia, a midline abdominal incision was performed and the bladder was exposed. A polyethylene catheter, the end of which had side holes (SP 10, Natsume Seisakusho, Japan), was inserted through the urethra and the contents inside the bladder were drained. Ten minutes after emptying the bladder, a perfusion fixation was performed through the left ventricle with 2% glutaraldehyde and 2% paraformaldehyde in 0.1 M phosphate buffer (PB; pH 7.4). After perfusion fixation, the bladder was cut into small pieces for embedding and fixed further for 1 h at room temperature in the same fixative. After washing with 0.1 M PB, post-fixation with 2% osmium tetroxide in 0.1 M PB was

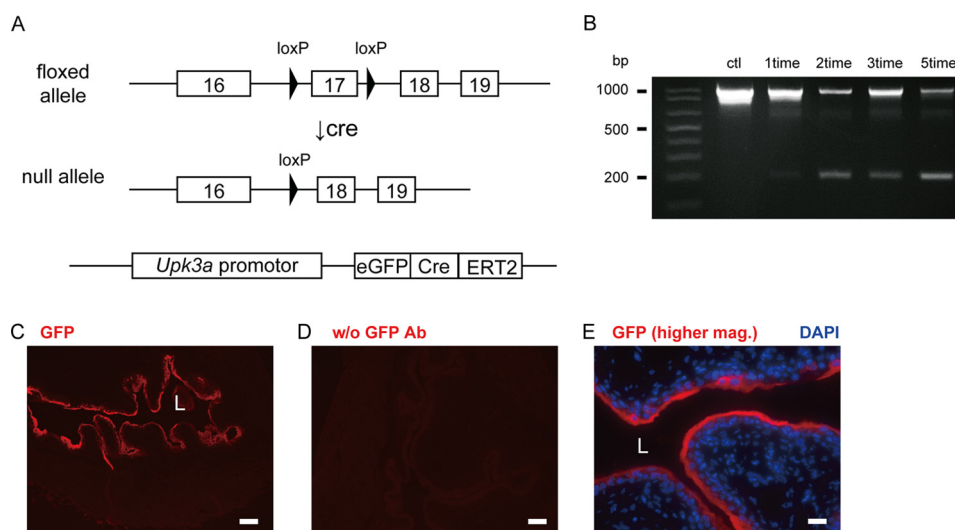


FIGURE 1. Generation of the urothelium-specific *Trpm7* KO mouse. *A*, this diagram shows our targeting strategy of the homologous recombination for the disruption of the *Trpm7* gene. Exon 17 of the *Trpm7* allele was flanked with two Lox P sites (arrowheads). Exon 17 encodes the protein sequence preceding the first transmembrane segment. The Cre-mediated deletion of exon 17 leads to a frameshift to translation without the channel and the kinase domain. The *Upk3a* promoter drives expression of the membrane protein called uroplakin 3a that is expressed only in urothelium. Thus, one can obtain urothelium-specific recombination by using this construct. Moreover, this construct also contains enhanced green fluorescent protein (eGFP), so in the transgenic mice, GFP should be expressed in cells that express uroplakin 3a. These mice were mated with the *Trpm7* flox mice to generate the double-positive mice. *B*, to confirm whether this Cre-loxP system worked correctly, PCR assessment of urothelial genomic DNA with or without tamoxifen was performed. In this PCR, the band of floxed *Trpm7* allele should be detected at around 1000-bp size, and the band of the null allele should be around 200 bp. Only the band of WT allele was found without tamoxifen (1st lane, *ctl*). After two or more administrations of tamoxifen, the band of the null allele was observed (2nd to 5th lanes). *C–E*, eGFP-positive cells were observed by immunohistochemistry using an anti-eGFP antibody to confirm the expression of Cre recombinase. Red signals indicate eGFP, and blue signals show DAPI. Signals were mainly found in the superficial layer of the urothelium with higher magnification (*E*). *D* shows a representative result without anti-eGFP antibody (*Ab*). Scale bars, 100 μ m (*C* and *D*) and 25 μ m (*E*). *L*, lumen.

performed for 1 h at room temperature. Dehydration in a graded ethanol series was followed by embedding samples in epoxy resin (Durcupan). Serial 70-nm-thick sections were cut from the sample surface orthogonally oriented to the epithelial cell layer and were collected in pioloform-coated single slot copper grids. Thin sections were stained with uranyl acetate and lead citrate and then observed with a JEM1010 transmission electron microscope (JEOL Co., Japan). Three images that had the widest intercellular junctions were selected from each mouse and the length between the surfaces of lateral cellular membranes was measured in each image.

Statistical Analysis—Data were analyzed using an unpaired *t* test or Mann-Whitney rank sum test. Values are shown as means \pm S.E. *p* values < 0.05 were considered significant.

Results

We first generated urothelium-specific *Trpm7* KO mice to reveal the functional significance of *Trpm7* in the urothelium. We used the promoter for the uroplakin 3a gene (*Upk3a*), the expression of which had been reported to be restricted to the urothelium (23, 24). Uroplakin is known to be a major component in the umbrella cells and makes a tight urothelial barrier (23, 25). First, we analyzed the actual promoter activity of the *Upk3a* gene in *Upk3a*-Cre mice by using an anti-eGFP antibody (Fig. 1*A*). The signal was indeed the highest in the superficial layer of the urothelium, modest in the intermediate, and lowest in the basal layer (Fig. 2, *C–E*). This outcome seemed to be suitable for the *Trpm7* KO because of their spatial expression patterns; by RT-PCR analysis, *Trpm7* mRNA was detected in the urothelium (Fig. 2*A*). When assessed by immunohistochemistry, *Trpm7* protein was also observed in the smooth

muscle layer. However, the expression level in the smooth muscle was lower than that in the urothelium (Fig. 2, *B–D*). In the urothelium, *Trpm7* protein was predominantly expressed in the superficial layer as reported previously (Fig. 2*D*) (26). This layer is composed of “umbrella cells” with long narrow rectangular shapes (13, 14). *Trpm7* protein was observed in the intermediate and basal layers of the urothelium as well, but expression levels were lower than in the superficial layer (Fig. 2*D*).

We then injected tamoxifen into these *Upk3a*-Cre;*Trpm7*^{fl/fl} double-positive mice to induce a urothelium-specific *Trpm7* KO (Fig. 1*A*). As shown in the genomic PCR with whole urothelium in Fig. 2*B*, intraperitoneal injections of tamoxifen indeed deleted exon 17 of the *Trpm7* gene in the urothelium, although the intact *Trpm7* genomic band was still present because we used whole urothelium. This deletion reportedly results in the production of a truncated *Trpm7* protein lacking both channel and kinase domains (7). We also confirmed that the quantity of *Trpm7* protein in the urothelium was significantly smaller after the application of tamoxifen but not in the detrusor, the smooth muscle layer (Fig. 2, *E–I*). These results indicated that urothelial *Trpm7* proteins were decreased by tamoxifen treatments.

Next, we established primary cultures of the urothelial cells. However, umbrella cells could not be maintained because they did not attach to culture dishes. However, we successfully isolated *Upk3a*-positive smooth muscle actin (*Acta2*)-negative cells that were most likely derived from the intermediate and basal layers of the urothelium (Fig. 3, *A* and *B*). In this culture, almost all of the cells were positive for cytokeratin 7 (CK7), an epithelial cell marker (Fig. 3*D*), but negative for cytokeratin 20 (CK20), an umbrella cell marker, on the 1st day of culture but

Functional Impairment of Urothelial *Trpm7*-Knock-out Bladder

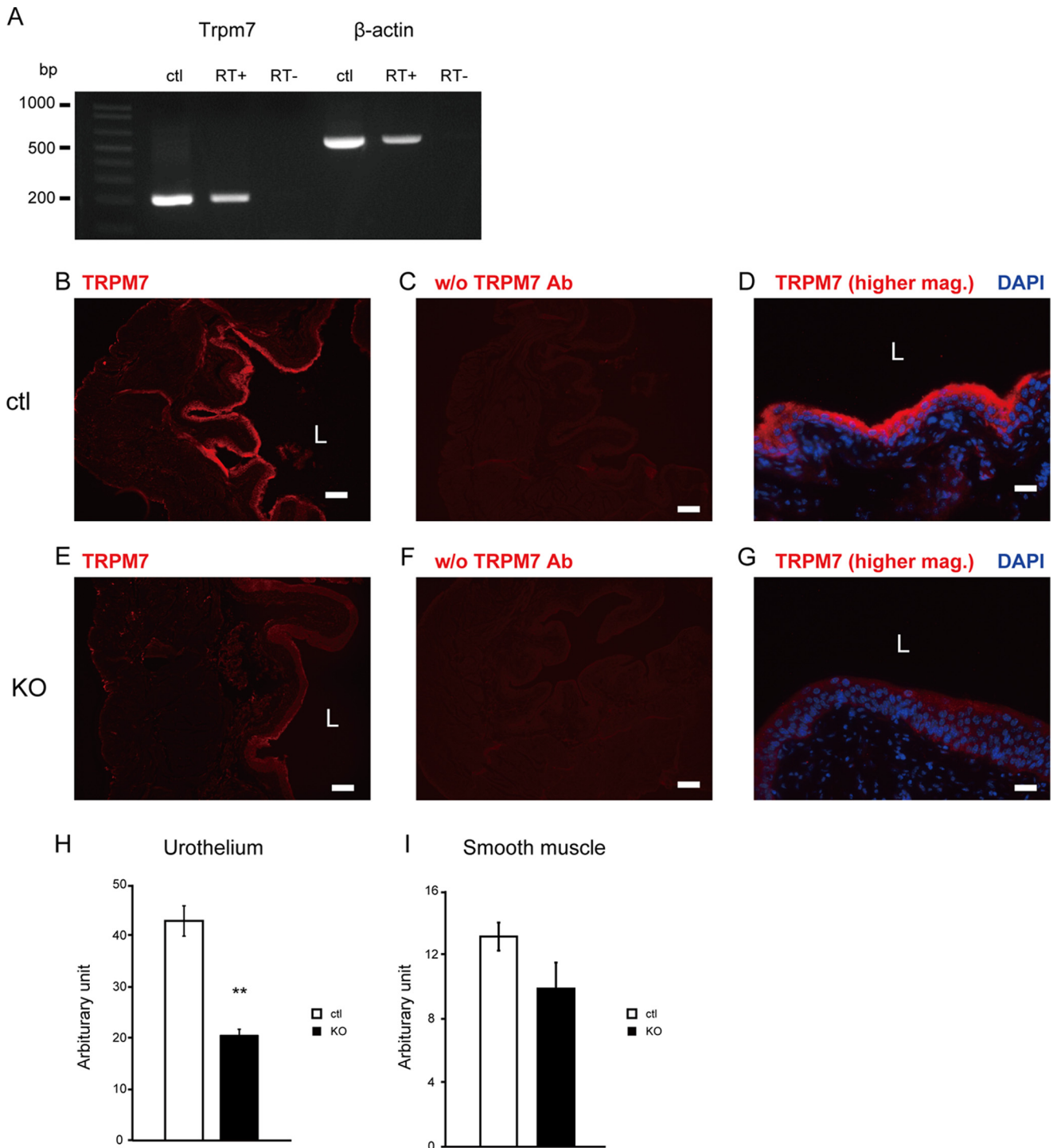


FIGURE 2. RT-PCR, PCR, and immunohistochemical assessment of TRPM7 in control and *Trpm7* KO urothelium. *A*, RT-PCR was performed to assess *Trpm7* mRNA expression in the bladder. *Trpm7* mRNA was found in the urothelium. *Ctl* lanes show a representative result of PCR analysis with a plasmid vector, including the partial cDNA of *Trpm7* or β -actin as a positive control. *B* and *D*, immunohistochemistry of TRPM7 in the whole bladder from control mice without tamoxifen treatment. Red signals indicate TRPM7 protein. The signal was predominantly found in the urothelium, especially the superficial layer. *E* and *G*, immunohistochemistry of TRPM7 in the tamoxifen-treated mouse bladder. The signal of TRPM7 was significantly attenuated by tamoxifen treatments compared with the control mice (*G*). *C* and *F*, control results without primary antibodies. Scale bars, 100 μ m (*B*, *C*, *E*, and *F*) and 25 μ m (*D* and *G*). *L*, lumen. *H* and *I*, quantification of *Trpm7* protein signals in the urothelium (*H*) or detrusor (smooth muscle layer) (*I*) using ImageJ software. *Trpm7* protein was significantly smaller in *Trpm7* KO urothelium but not in the detrusor (**, $p < 0.01$, six different mice, Mann-Whitney test).

partially positive on the 2nd and 3rd days of the culture (data not shown). This strongly suggested that these cells were urothelial cells from the intermediate or basal layer of the urothelium. Moreover, *Trpm7* protein was colocalized with CK7 (Fig. 3, *C–E*), and *Trpm7* protein signals were confirmed

to be reduced by tamoxifen treatments without changes in CK7 signals (Fig. 3, *F–H*).

Using this culture system, we performed whole-cell patch clamp recordings. Because it had been reported that physiological concentrations of Mg^{2+} inhibited *Trpm7* activity, we used

Functional Impairment of Urothelial *Trpm7*-Knock-out Bladder

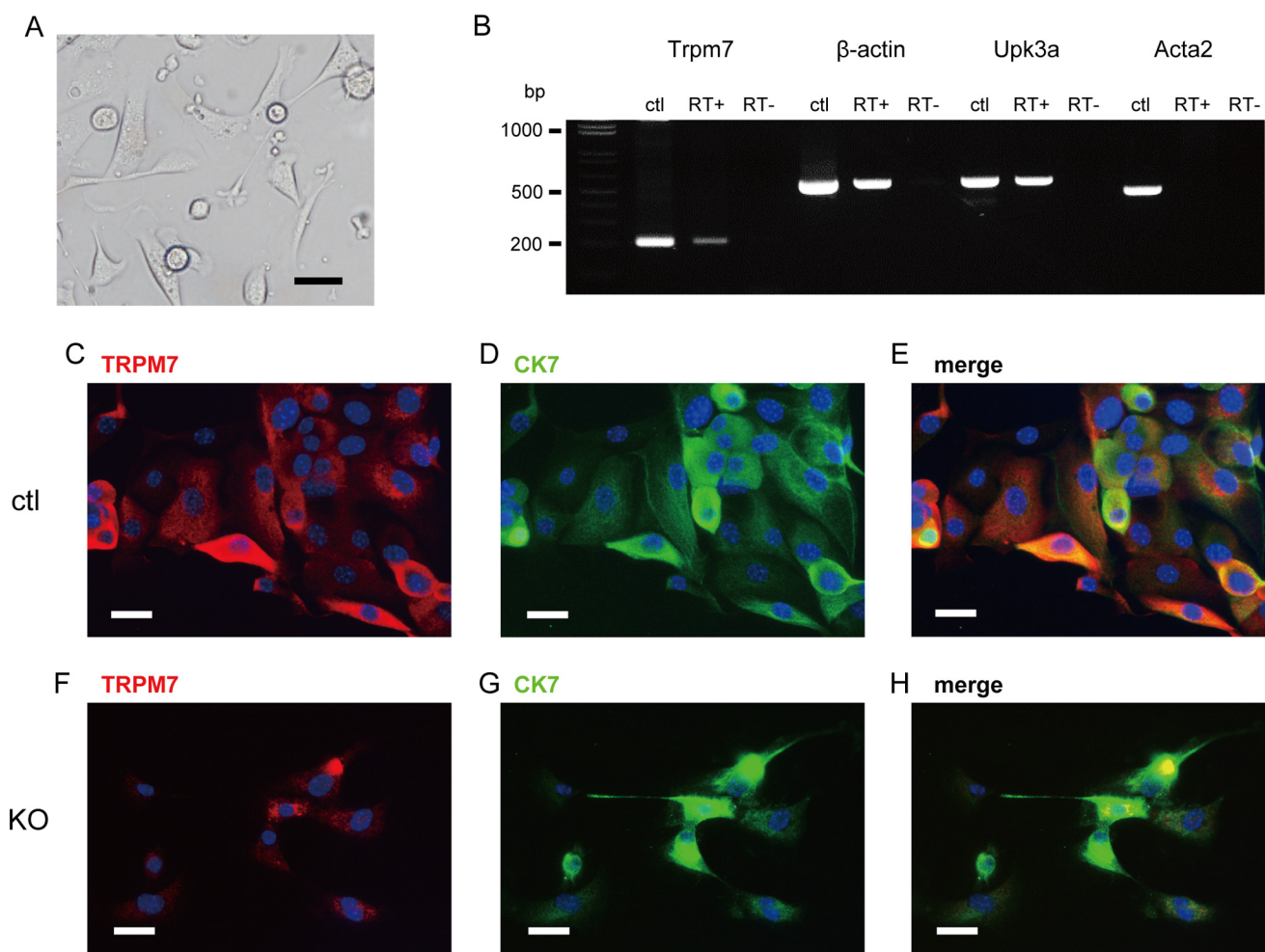
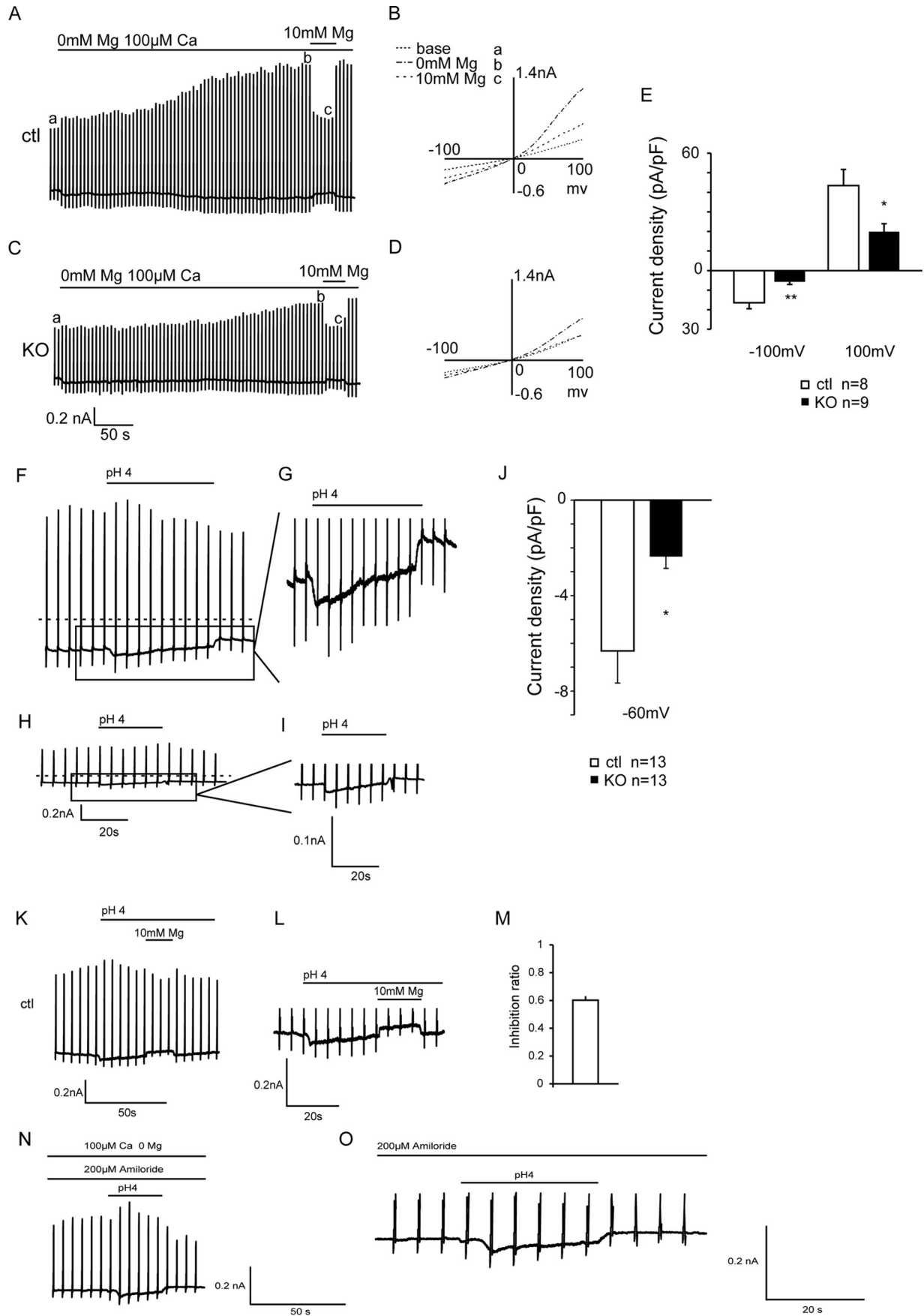


FIGURE 3. Isolation of primary urothelial cells. *A*, bright field image of the isolated primary urothelial cells from control mouse. These cells are firmly adhesive on the surface of the dish. There were also round-shaped cells with insufficient attachment. *Scale bar*, 50 μm . *B*, representative result of RT-PCR in the isolated mouse urothelial cell culture. The band for *Trpm7* (209 bp) was detected. *Upk3a* (606 bp), a urothelial marker, was also found, but *Acta2* (503 bp), a smooth muscle marker, was not found. *Ctl lanes* indicate a representative result of PCR with a plasmid vector, including the partial cDNA of *Trpm7*, β -actin, *Upk3a*, or *Acta2* as a positive control. *C–E*, immunocytochemistry of primary urothelial cells from a control mouse. *Trpm7* (red, *C* and *E*) was observed, colocalizing with an epithelial cell marker CK7 (green, *D* and *E*). *Scale bars*, 25 μm . *F–H*, immunocytochemistry of TRPM7 (*F* and *H*) and CK7 (*G* and *H*) in primary urothelial cells isolated from *Trpm7* KO mice with tamoxifen treatments. The TRPM7 signals were significantly reduced without changes in CK7 signals.

extracellular and intracellular Mg^{2+} -free conditions (27). After starting incubation with 0 mM Mg^{2+} and 100 μM Ca^{2+} , membrane currents with an outwardly rectifying property were significantly increased, and these currents were gradually increased further during the incubation with the same bath solution (Fig. 4, *A* and *B*). The increase of these currents usually lasted ~ 5 min. All these characteristics were similar to those reported for *Trpm7* currents (Mg^{2+} -inhibitable current) (27). Indeed, these currents were significantly smaller when cells isolated from tamoxifen-treated mice were used (-5.7 ± 1.3 pA/pF in KO and -16.4 ± 3.0 pA/pF in control, holding at -100 mV, $p < 0.01$; 19.9 ± 4.0 pA/pF in KO and 43.4 ± 8.3 pA/pF in control, holding at $+100$ mV, $p < 0.03$, $n = 8-9$) (Fig. 4, *C–E*). These results indicated that *Trpm7* channels were functionally expressed in urothelial cells, as shown in the previous report (15), and that functional *Trpm7* channels were actually decreased by tamoxifen treatments, again supporting the supposition that the *Trpm7* KO mice had been generated properly.

Another characteristic of *Trpm7* currents is its pH dependence (28, 29). *Trpm7* currents are reportedly activated by extracellular acid loading due to the competition between H^+ and Mg^{2+} , and this effect was observed only in inward currents (29). In our hands, the increase in inward currents by acid (Fig. 4, *F* and *G*) and their inhibition by Mg^{2+} (10 mM) (Fig. 4, *K–M*) were confirmed. Importantly, these acid-induced inward currents were significantly smaller when cells isolated from tamoxifen-treated mice were used (-2.4 ± 0.49 pA/pF in KO and -6.3 ± 1.35 pA/pF in control, holding at -100 mV, $p < 0.03$, $n = 13$) (Fig. 4, *H–J*), suggesting that endogenous acid-sensitive currents were derived at least in part from *Trpm7*. To exclude the possibility that acid-evoked currents were derived from other channels such as acid-sensing ion channels, TRPV1, TRPA1 or TRPV4, we first performed Ca^{2+} imaging with application of capsaicin (TRPV1 agonist) or allyl isothiocyanate (TRPA1 agonist). There was no significant increase in intracellular Ca^{2+} concentration (data not shown). These results suggested there might be a small contribution of TRPV1 or TRPA1

Functional Impairment of Urothelial Trpm7-Knock-out Bladder



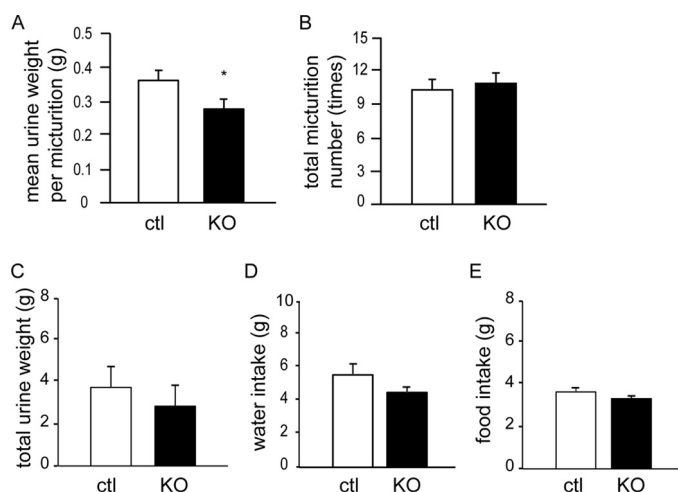


FIGURE 5. **Voiding behavior.** In *Trpm7* KO mice, mean voided volume was significantly smaller compared with the control mice (*, $p < 0.05$, $n = 6-8$) (A). The mean value of total micturition number was higher in KO mice but not statistically significant (B). There was no significant difference in total urine weight (C), water intake (D), or food intake (E) between the two genotypes.

in urothelial cells under these conditions. Next, we carried out patch clamp recordings to further investigate acid-evoked currents. Neither amiloride (acid-sensing ion channel inhibitor) nor HC067047 (TRPV4 antagonist) inhibited acid-evoked currents (Fig. 4, *N* and *O*, for amiloride and data not shown for HC067047). These results supported our hypothesis that *Trpm7*-derived acid-sensitive currents are present in native urothelial cells.

Our main purpose was to reveal whether urothelial *Trpm7* contributed to the *in vivo* function of the bladder. We analyzed the voiding behavior of free-moving mice by using metabolic cages (30) and found a significant difference in the urine voided volume between control (tamoxifen-injected *Trpm7*^{fl/fl} mice) and *Trpm7* KO mice (tamoxifen-injected *Upk3a-Cre;Trpm7*^{fl/fl} mice). The voided volume was significantly smaller in *Trpm7* KO mice than controls (mean voided volume 0.28 ± 0.08 g in KO mice versus 0.36 ± 0.04 g in control mice, $p = 0.03$, $n = 6-8$, Mann-Whitney test) (Fig. 5A). There was no significant difference in total micturition number ($p = 0.65$, $n = 6-8$), urine weight ($p = 0.36$, $n = 6-8$), or water and food intake ($p = 0.22$ and 0.16 , $n = 6-8$) between the two genotypes (Fig. 5, B–E). There was no difference in urine osmolarity either (1651.6 ± 268.9 mosm/kg H₂O in controls, 2156.7 ± 222.5 mosm/kg H₂O in *Trpm7* KO mice, $p = 0.24$, $n = 6$, Mann-Whitney test).

Next, we investigated why the voided volume was decreased. We performed histological analysis of hematoxylin and eosin-stained tissues. As shown in Fig. 6B, partial but substantial edema in the submucosal layer was observed in tamoxifen-in-

jected *Trpm7* KO bladders but not in control (Fig. 6A). We found that the edema scores were significantly higher in the *Trpm7* KO mice (2.43 ± 0.43 versus 0.75 ± 0.37 , $p < 0.05$, $n = 7-8$) (Fig. 6C). These results suggested that interstitial inflammation led to the decreased voided volume. Moreover, we performed quantitative PCR analysis of the expression of various cytokines (*Tnfa*, *Il1b*, *Il6*, *Il10*, *Il12*, *Il15*, *Il18*, and *Tgfb1*). Among these cytokines, mRNA expression of proinflammatory cytokines *Tnfa* and *Il1b* was significantly higher in *Trpm7* KO bladders than in the bladders from Cre-negative tamoxifen-treated control mice (Fig. 6, D and E). These results supported our idea that loss of urothelial *Trpm7* resulted in submucosal inflammation.

We hypothesized that *Trpm7* was important to the formation of intercellular junctions (9–12) and that *Trpm7* KO might lead to the disruption of intercellular junctions, resulting in impaired epithelial barrier function and inflammation. Therefore, we investigated the microarchitecture of the urothelium by electron microscopy. We found that the intercellular junctions of the superficial layer of the urothelium differed between control and *Trpm7* KO mice (Fig. 7, A–D). When focusing on the apical junction complex with surrounding intracellular dense filaments, which were most likely adherens junctions, the extra space between the urothelial cells in *Trpm7* KO mice was significantly larger compared with controls (43.2 and 17.1 nm, respectively, $p < 0.01$, $n = 12-15$, Fig. 7E). It seemed that the tightness of the intercellular junction in the superficial layer of the urothelium was looser in *Trpm7* KO mice than in control mice. No changes in other structures were observed, including intracellular vesicles. These results suggested that *Trpm7* was involved in the formation of intercellular junction in mouse urothelium.

Discussion

In this study, we found that *Trpm7* was expressed in the urothelium, especially the superficial layer, and that endogenous *Trpm7* elicited acid-evoked currents. When *Trpm7* in the superficial layer of the urothelium was knocked out, we observed immature intercellular junctions in the superficial layer, substantial inflammation in the submucosal layer, and significantly smaller voided volume. Overactive bladder that is defined as urine storage symptoms, including urgency and frequency, has been attributed to urothelial, smooth muscle, or neurogenic mechanisms. In terms of the urothelial mechanism, although it has been believed that several transmitters (e.g. ATP and NO) secreted from urothelial cells play a role in the over-activation of the urinary bladder via its primary sensory neurons, the detailed mechanism is still unknown. By using *in vivo* analysis, we found a decreased voided volume in *Trpm7* KO

FIGURE 4. **Whole-cell patch clamp recordings in mouse primary urothelial cells.** A and B, currents observed when pipette and extracellular solutions did not contain magnesium. A, in the case of urothelial cells from a control mouse, the outward rectifying current increased with time. When magnesium (10 mM) was added to bath solution, these currents were inhibited. After changing to 0 mM magnesium solution, the currents became larger again. These properties as well as the current-voltage relationship (B) were similar to those of reported magnesium-inhibitable cation currents derived from TRPM7. C and D, in the case of urothelial cells from a *Trpm7* KO mouse with tamoxifen treatments, the above mentioned currents were significantly smaller compared with the control mice (E) ($p < 0.03$, $n = 8-9$). *, $p < 0.03$; **, $p < 0.01$. whole-cell patch clamp recordings in urothelial cells from control mouse. When cells were exposed to the acidic solution (pH 4), inward currents were potentiated, and these currents were inhibited by 10 mM magnesium (K–M). Acid-evoked currents (H and I) were significantly smaller in *Trpm7* KO mice with tamoxifen treatments than those of control mice (J) ($p < 0.03$, $n = 13$). Dotted lines indicate zero-current levels. N and O, representative time traces of acid (pH 4)-evoked currents with amiloride in whole-cell patch clamp recordings. The acid-sensing ion channel inhibitor amiloride (200 μ M) did not inhibit the current.

Functional Impairment of Urothelial *Trpm7*-Knock-out Bladder

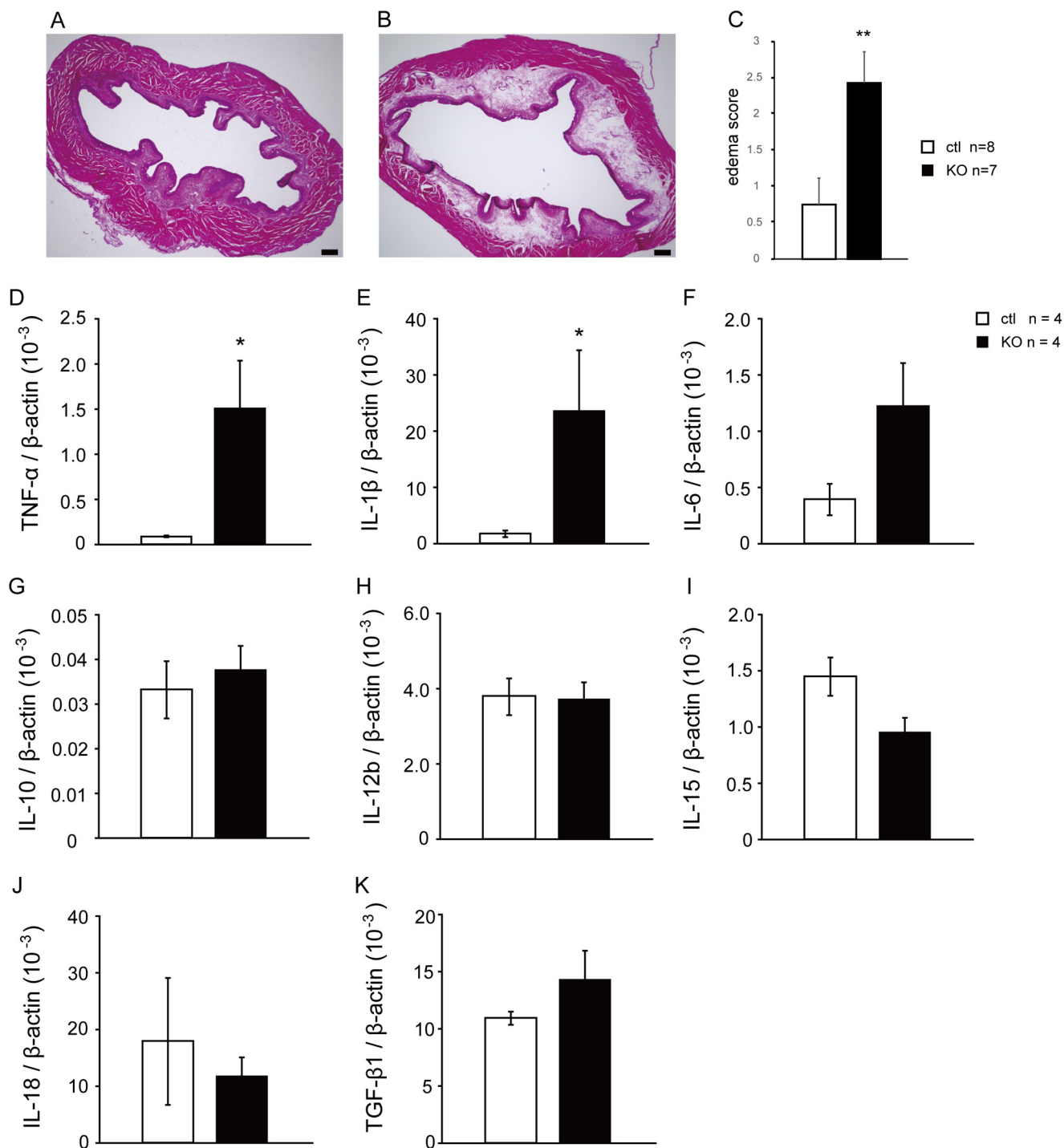


FIGURE 6. Histological analysis and cytokine profile of mouse bladder. A representative result of hematoxylin and eosin staining of control (A) or *Trpm7* KO (B) bladders. Substantial edema was observed in the submucosal layer of *Trpm7* KO bladder but not in the control. C, edema scores were significantly larger in *Trpm7* KO bladder ($p < 0.05$, $n = 7-8$). D-K, quantitative PCR results of cytokines in control or *Trpm7* KO bladder. Proinflammatory cytokines TNF- α (D) and IL-1 β (E) were significantly higher in *Trpm7* KO bladder ($p < 0.03$, $n = 4$, Mann-Whitney test). *, $p < 0.03$; **, $p < 0.05$.

mice. We hypothesize that the smaller voided volume is due to the formation of immature tight junctions, resulting in an increased urothelial permeability, which in turn could cause inflammation and an overactive bladder.

One example of this kind of phenomenon is observed in autoimmune responses against urothelial proteins (31) or umbrella cell-specific proteins (32) that could cause submucosal inflammation. Other reports showed that immature intercellular junctions

caused by p120 catenin KO (33) or dominant-negative N-cadherin (34) affected epithelial barrier function followed by inflammation in the small intestine. We hypothesize that our urothelial *Trpm7*-knockdown mice follow a similar pathogenic course.

A remaining question is the mechanism by which the lack of *Trpm7* leads to abnormal intercellular junction formation. Previously, it was reported that TRPV4 was involved in intercellular junction formation in mouse epidermal keratinocytes (35).

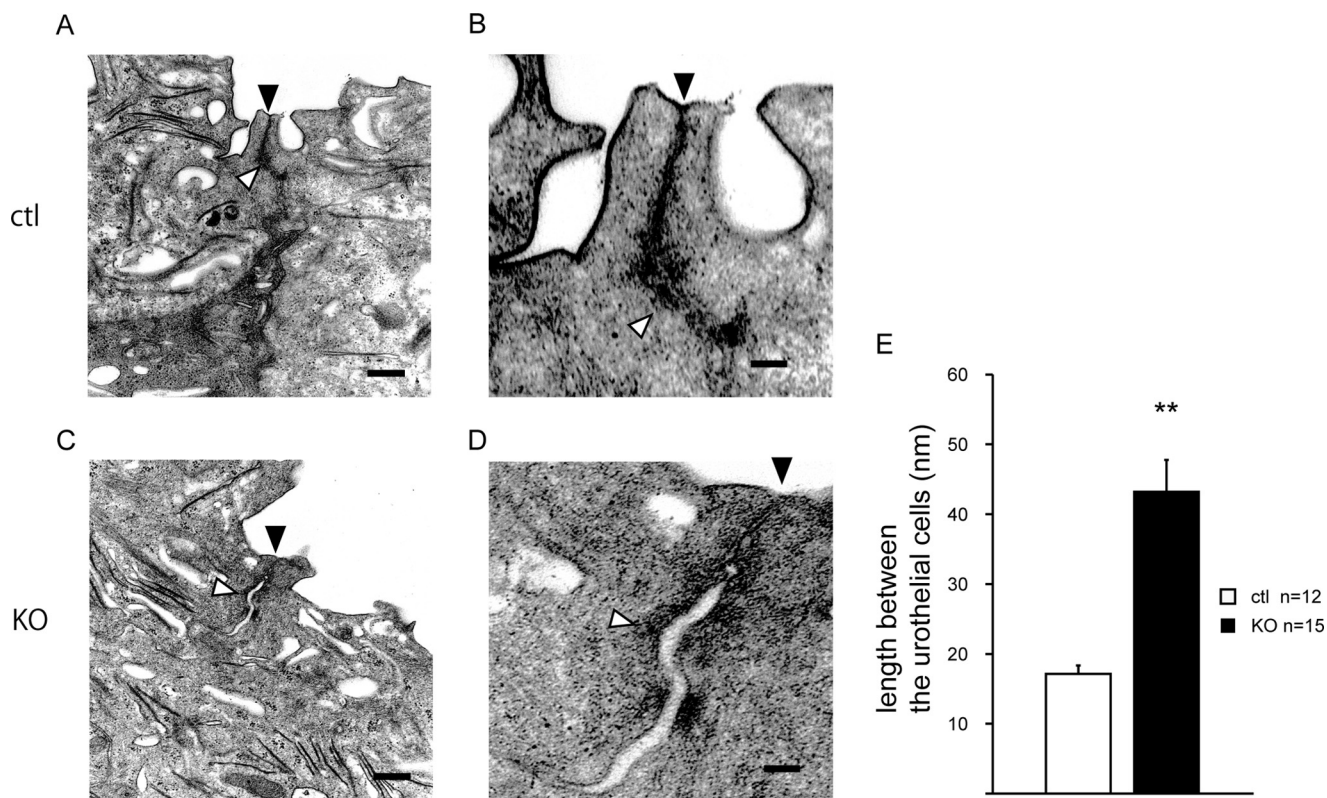


FIGURE 7. **Transmission electron microscopy of the mouse urothelium.** Representative images of transmission electron microscopy of the intercellular junction of the superficial layer of the urothelial cells from control mice (A and B) or *Trpm7* KO mice (C and D). Black arrowheads indicate tight junctions, and white arrowheads indicate the end of junction complexes containing adherens junctions. There was a significant difference in the width of the intercellular space of the basal side between control and *Trpm7* KO mice (E) (17.1 and 43.2 nm, respectively, **, $p < 0.01$, $n = 12-15$). Scale bars, 200 nm (A and C) and 50 nm (B and D).

TRPV4 is another non-selective cation channel that can be activated by warm temperature or hypo-osmolarity. Sokabe *et al.* (35) showed that TRPV4 activation triggered intracellular Ca^{2+} increase, followed by the activation of Rho GTPase, which is a key component for keratinocyte differentiation, resulting in actin organization and intercellular junction formation. When TRPV4 was inhibited by ruthenium red, keratinocytes formed weaker stress fibers. Similar to the case of keratinocyte TRPV4, we speculate that the differentiation process of umbrella cells might be attenuated in the *Trpm7* KO.

In the case of TRPV4, warm temperature could be a good candidate for the environmental stimulus that induces epidermal keratinocyte differentiation. Thus, one can ask what kind of stimulus activates *Trpm7* to induce umbrella cell differentiation. Our hypothesis is that environmental (urinary) acid or hypotonic stress stimulates *Trpm7* to induce the maturation of umbrella cells. The turnover rate of umbrella cells has been reported to be extremely long (3–6 months) (13). However, surprisingly, when cells in the intermediate layer of the urothelium were exposed to the outside milieu, they started to differentiate into umbrella cells within days after damage and that is the mechanism by which the urothelial barrier function is maintained. Thus, we speculate that urothelial cells somehow receive information from their surrounding environment. The (molecular) identity of the signaling mechanism has not yet been identified. We would like to propose that acid or osmolarity change is recognized by *Trpm7* in intermediate or basal urothelial

cells, and this might trigger their differentiation into mature umbrella cells. Future studies should reveal factors for umbrella cell differentiation and involvement of *Trpm7* in this process.

Some TRP channels have been reported to form a complex with other signaling proteins and/or cytoskeletal proteins. Because there is no evidence showing the involvement of *Trpm7* channel activity with the *in vivo* phenotype, other possibilities cannot be excluded. *Trpm7* might contribute to the intercellular junction formation as a scaffolding protein. In cancer cells, it has been reported that *Trpm7* associates with myosin and phosphorylates it by its kinase domain in the C terminus, which is involved in intercellular junction formation (12). TRPV4 has been reported to be involved in intracellular junction formation, directly associating with E-cadherin and β -catenin, which are the major players of adherens junction (35). Future work using channel-dead or kinase-dead *Trpm7* knock-in mice might be suitable to address the question whether the channel or kinase activity of *Trpm7* is involved in the *in vivo* phenotype.

Author Contributions—M. W. and Y. S. designed the study and performed the experiments. K. U. analyzed the data. N. M. and K. M. provided technical assistance and contributed to the electron microscopy study. K. U., S. M., H. K., and M. T. contributed to the data discussion. M. W., Y. S., and M. T. wrote the paper. All authors reviewed the results and approved the final version of the manuscript.

Acknowledgments—We greatly thank Dr. D. E. Clapham (Children's Hospital, Boston) for *Trpm7*-floxed mice and Dr. Y. Mori (Kyoto University, Japan) for rabbit anti-TRPM7 antibody. We also thank Drs. M. Takeda, T. Mochizuki, and T. Miyamoto (University of Yamaguchi, Japan) for their technical advice for the primary urothelial cells and Naomi Fukuta, Claire T. Saito, and Sachiko Yamada for their technical assistance. We also appreciate Dr. T. Numata (Kyoto University, Japan) for advice regarding patch clamp recordings for *Trpm7*.

References

- Julius, D. (2013) TRP channels and pain. *Annu. Rev. Cell Dev. Biol.* **29**, 355–384
- Ramsey, I. S., Delling, M., and Clapham, D. E. (2006) An introduction to TRP channels. *Annu. Rev. Physiol.* **68**, 619–647
- Venkatachalam, K., and Montell, C. (2007) TRP channels. *Annu. Rev. Biochem.* **76**, 387–417
- Voets, T., Talavera, K., Owsianik, G., and Nilius, B. (2005) Sensing with TRP channels. *Nat. Chem. Biol.* **1**, 85–92
- Fleig, A., and Chubanov, V. (2014) *Trpm7*. *Handb. Exp. Pharmacol.* **222**, 521–546
- Ryazanova, L. V., Rondon, L. J., Zierler, S., Hu, Z., Galli, J., Yamaguchi, T. P., Mazur, A., Fleig, A., and Ryazanov, A. G. (2010) TRPM7 is essential for Mg²⁺ homeostasis in mammals. *Nat. Commun.* **1**, 109
- Jin, J., Desai, B. N., Navarro, B., Donovan, A., Andrews, N. C., and Clapham, D. E. (2008) Deletion of *Trpm7* disrupts embryonic development and thymopoiesis without altering Mg²⁺ homeostasis. *Science* **322**, 756–760
- Jin, J., Wu, L. J., Jun, J., Cheng, X., Xu, H., Andrews, N. C., and Clapham, D. E. (2012) The channel kinase, TRPM7, is required for early embryonic development. *Proc. Natl. Acad. Sci. U.S.A.* **109**, E225–E233
- Clark, K., Langeslag, M., van Leeuwen, B., Ran, L., Ryazanov, A. G., Figdor, C. G., Moolenaar, W. H., Jalink, K., and van Leeuwen, F. N. (2006) TRPM7, a novel regulator of actomyosin contractility and cell adhesion. *EMBO J.* **25**, 290–301
- Clark, K., Middelbeek, J., and van Leeuwen, F. N. (2008) Interplay between TRP channels and the cytoskeleton in health and disease. *Eur. J. Cell Biol.* **87**, 631–640
- Su, L. T., Agapito, M. A., Li, M., Simonson, W. T., Huttenlocher, A., Habas, R., Yue, L., and Runnels, L. W. (2006) TRPM7 regulates cell adhesion by controlling the calcium-dependent protease calpain. *J. Biol. Chem.* **281**, 11260–11270
- Middelbeek, J., Kuipers, A. J., Henneman, L., Visser, D., Eidhof, I., van Horssen, R., Wieringa, B., Canisius, S. V., Zwart, W., Wessels, L. F., Sweep, F. C., Bult, P., Span, P. N., van Leeuwen, F. N., and Jalink, K. (2012) TRPM7 is required for breast tumor cell metastasis. *Cancer Res.* **72**, 4250–4261
- Khandelwal, P., Abraham, S. N., and Apodaca, G. (2009) Cell biology and physiology of the uroepithelium. *Am. J. Physiol. Renal Physiol.* **297**, F1477–F1501
- Minsky, B. D., and Chlapowski, F. J. (1978) Morphometric analysis of the translocation of luminal membrane between cytoplasm and cell surface of transitional epithelial cells during the expansion-contraction cycles of mammalian urinary bladder. *J. Cell Biol.* **77**, 685–697
- Everaerts, W., Vriens, J., Owsianik, G., Appendino, G., Voets, T., De Ridder, D., and Nilius, B. (2010) Functional characterization of transient receptor potential channels in mouse urothelial cells. *Am. J. Physiol. Renal Physiol.* **298**, F692–F701
- Hayashi, S., and McMahon, A. P. (2002) Efficient recombination in diverse tissues by a tamoxifen-inducible form of Cre: a tool for temporally regulated gene activation/inactivation in the mouse. *Dev. Biol.* **244**, 305–318
- Miyamoto, T., Mochizuki, T., Nakagomi, H., Kira, S., Watanabe, M., Takayama, Y., Suzuki, Y., Koizumi, S., Takeda, M., and Tominaga, M. (2014) Functional role for Piezo1 in stretch-evoked Ca²⁺ influx and ATP release in urothelial cell cultures. *J. Biol. Chem.* **289**, 16565–16575
- Mochizuki, T., Sokabe, T., Araki, I., Fujishita, K., Shibasaki, K., Uchida, K., Naruse, K., Koizumi, S., Takeda, M., and Tominaga, M. (2009) The TRPV4 cation channel mediates stretch-evoked Ca²⁺ influx and ATP release in primary urothelial cell cultures. *J. Biol. Chem.* **284**, 21257–21264
- Gevaert, T., Vriens, J., Segal, A., Everaerts, W., Roskams, T., Talavera, K., Owsianik, G., Liedtke, W., Daelemans, D., Dewachter, I., Van Leuven, F., Voets, T., De Ridder, D., and Nilius, B. (2007) Deletion of the transient receptor potential cation channel TRPV4 impairs murine bladder voiding. *J. Clin. Invest.* **117**, 3453–3462
- Everaerts, W., Zhen, X., Ghosh, D., Vriens, J., Gevaert, T., Gilbert, J. P., Hayward, N. J., McNamara, C. R., Xue, F., Moran, M. M., Strassmaier, T., Uykai, E., Owsianik, G., Vennekens, R., De Ridder, D., et al. (2010) Inhibition of the cation channel TRPV4 improves bladder function in mice and rats with cyclophosphamide-induced cystitis. *Proc. Natl. Acad. Sci. U.S.A.* **107**, 19084–19089
- Apodaca, G., Kiss, S., Ruiz, W., Meyers, S., Zeidel, M., and Birder, L. (2003) Disruption of bladder epithelium barrier function after spinal cord injury. *Am. J. Physiol. Renal Physiol.* **284**, F966–F976
- Beppu, K., Sasaki, T., Tanaka, K. F., Yamanaka, A., Fukazawa, Y., Shigemoto, R., and Matsui, K. (2014) Optogenetic countering of glial acidosis suppresses glial glutamate release and ischemic brain damage. *Neuron* **81**, 314–320
- Kreft, M. E., Jezernik, K., Kreft, M., and Romih, R. (2009) Apical plasma membrane traffic in superficial cells of bladder urothelium. *Ann. N.Y. Acad. Sci.* **1152**, 18–29
- Gandhi, D., Molotkov, A., Batourina, E., Schneider, K., Dan, H., Reiley, M., Laufer, E., Metzger, D., Liang, F., Liao, Y., Sun, T. T., Aronow, B., Rosen, R., Mauney, J., Adam, R., et al. (2013) Retinoid signaling in progenitors controls specification and regeneration of the urothelium. *Dev. Cell* **26**, 469–482
- Hu, P., Deng, F. M., Liang, F. X., Hu, C. M., Auerbach, A. B., Shapiro, E., Wu, X. R., Kachar, B., and Sun, T. T. (2000) Ablation of uroplakin III gene results in small urothelial plaques, urothelial leakage, and vesicoureteral reflux. *J. Cell Biol.* **151**, 961–972
- Yu, W., Hill, W. G., Apodaca, G., and Zeidel, M. L. (2011) Expression and distribution of transient receptor potential (TRP) channels in bladder epithelium. *Am. J. Physiol. Renal Physiol.* **300**, F49–F59
- Nadler, M. J., Hermosura, M. C., Inabe, K., Perraud, A. L., Zhu, Q., Stokes, A. J., Kurosaki, T., Kinet, J. P., Penner, R., Scharenberg, A. M., and Fleig, A. (2001) LTRPC7 is a Mg-ATP-regulated divalent cation channel required for cell viability. *Nature* **411**, 590–595
- Jiang, J., Li, M., and Yue, L. (2005) Potentiation of TRPM7 inward currents by protons. *J. Gen. Physiol.* **126**, 137–150
- Numata, T., and Okada, Y. (2008) Proton conductivity through the human TRPM7 channel and its molecular determinants. *J. Biol. Chem.* **283**, 15097–15103
- Wood, R., Eichel, L., Messing, E. M., and Schwarz, E. (2001) Automated noninvasive measurement of cyclophosphamide-induced changes in murine voiding frequency and volume. *J. Urol.* **165**, 653–659
- Sugino, Y., Nishikawa, N., Yoshimura, K., Kuno, S., Hayashi, Y., Yoshimura, N., Okazaki, T., Kanematsu, A., and Ogawa, O. (2012) BALB/c-Fcgr2bPdcd1 mouse expressing anti-urothelial antibody is a novel model of autoimmune cystitis. *Sci. Rep.* **2**, 317
- Izgi, K., Altuntas, C. Z., Bicer, F., Ozer, A., Sakalar, C., Li, X., Tuohy, V. K., and Daneshgari, F. (2013) Uroplakin peptide-specific autoimmunity initiates interstitial cystitis/painful bladder syndrome in mice. *PLoS ONE* **8**, e72067
- Smalley-Freed, W. G., Efimov, A., Burnett, P. E., Short, S. P., Davis, M. A., Gumucio, D. L., Washington, M. K., Coffey, R. J., and Reynolds, A. B. (2010) p120-catenin is essential for maintenance of barrier function and intestinal homeostasis in mice. *J. Clin. Invest.* **120**, 1824–1835
- Hermiston, M. L., and Gordon, J. I. (1995) Inflammatory bowel disease and adenomas in mice expressing a dominant-negative N-cadherin. *Science* **270**, 1203–1207
- Sokabe, T., Fukumi-Tominaga, T., Yonemura, S., Mizuno, A., and Tominaga, M. (2010) The TRPV4 channel contributes to intercellular junction formation in keratinocytes. *J. Biol. Chem.* **285**, 18749–18758